Diet-induced miRNAs regulate adult neurogenesis and functional activity of nascent neurons in the hypothalamus.

Balakumar Srinivasan[1], Sarbani Samaddar[1], Dipanjan Roy[1,2] and Sourav Banerjee[1]

1. National Brain Research Centre, NH8, Nainwal Mode, Manesar 122052, Haryana, INDIA
2. Current address: School of Artificial Intelligence and Data Science, Indian Institute of Technology, Jodhpur 342030, Rajasthan, INDIA

Correspondence: souravnbrc@gmail.com or sourav@nbrc.ac.in

Abstract:

Neurogenesis in the hypothalamus upon high fat diet (HFD) feeding regulates the feeding circuit. HFD induces the neurogenesis of β2 tanycytes in young- adult mice. However molecular mechanisms of tanycytic neurogenesis; and their functional integration into the feeding circuitry are poorly understood. We investigated the role of miRNAs in the regulation of HFD-induced tanycytic neurogenesis. miRNA arrays identified a cohort of HFD-induced, differentially-regulated miRNAs in $BrdU^+$ β2-tanycytes. These miRNAs arise from different chromosomes, rather than a single cluster. *In silico* network analysis on the predicted targets of all five HFD-induced miRNAs and reporter assays identified a subset of targets that influence neurogenesis and neuronal differentiation. HFD-induced miRNAs drive a molecular program leading to the functional integration of nascent neurons; introduction of a miRNA sponge sequestering all five miRNAs abolishes it. Diet-regulated newborn neurons preferentially differentiate into AgRP+ neurons that functionally integrate into the feeding circuit.

Introduction:

Hypothalamic adult neurogenesis in response to acute or sustained dietary changes modulate long-term physiological responses in the body (*1*, *2*) manifesting as gain in body weight has been observed in mice for both acute and chronic high fat diet (HFD) feeding paradigms. While chronic administration of HFD led mice to develop severe forms of obesity (*3*, *4*); acute HFD feeding led to reversible forms of obesity (*5*). The neurogenic patterns and the source niches of such differential feeding paradigms are markedly different as they are modulated to meet the physiological metabolic demands due to the dietary factors (*6*) Acute HFD feeding paradigms induce the genesis of nascent neurons in the median eminence of the hypothalamus in adult mice (*2*). The median eminence (MEm) of the hypothalamus has an active neurogenic zone marked by the presence of Nestin positive, radial glia-like ependymal cells like tanycytes (*7*).

Tanycytes are metabolite sensing cells lining the ventral third ventricular wall. They are anatomically characterized into α1-, α2- , β1- , β2- tanycytes and have characteristically long projections to the dorsomedial hypothalamus, ventromedial hypothalamus, arcuate nucleus (ARC) and the median eminence (MEm) (*7*). These unique ependymal cells are of particular interest because of their ability to sense metabolites from the cerebrospinal fluid and the blood, as they exist outside the blood brain barrier (*7*). Specifically, β1- and β2- tanycytes project these signals to activate the feeding circuit in the arcuate nucleus of the hypothalamus. β2-tanycytes are $Sox2^+$, $Nestin^+$, and $Vimentin^+$ neural progenitor cells that adapt to a neural fate in response to changes in dietary factors (*2*). Neurogenesis from β2-tanycytes is vital to the metabolic changes incurred in response to HFD in female mice. Focal irradiation of the median eminence causes the abrogation of

β2-tanycytes that leads to decreased weight gain (*2*) in spite of a HFD feeding paradigm, thereby establishing a causal relationship between tanycytic neurogenesis and HFD-induced weight gain.

Feeding neural circuit in the mouse brain is centralized at the arcuate nucleus (ArcN) of the hypothalamus, which consists of both anorexigenic neurons and orexigenic neurons. The anorexigenic neurons inhibits feeding behaviour in response to satiety signals and are characterized by the expression of proopiomelanocortin (POMC), while the orexigenic neurons promote feeding behaviour in response to hunger signals and are characterized by the expression of Agouti-related peptide (AgRP) (*8*–*10*). Their activities are dimorphic and they inhibit each other (*10*). However, there is little knowledge as to how HFD-induced neurogenesis from β2-tanycytes functionally integrates into the feeding circuitry and how these nascent neurons influence AgRP or POMC activity in the ARC.

Among various regulatory molecules underlying diet-induced modulation of the feeding circuitry in the hypothalamus, miRNAs play a unique yet understudied role. miRNAs are small noncoding RNAs that have the ability to regulate the translational fate of their cognate mRNAs in response to external stimuli. Therefore, it is a valid extrapolation that miRNAs may control the translation of several key mRNAs associated with metabolic pathways during both acute and chronic dietary changes. Indeed, there are several studies that document changes in hypothalamic miRNA expression profile within rats in response to both short and long term changes in their nutritional intake (*11*, *12*). Calorie restriction or HFD feeding affected the expression of the miRNAs let-7a, miR-9, miR-30e, miR-132, miR-145, miR-200a and miR-218. Another miRNA; miR-103, was found to regulate hyperphagic obesity in Dicer knockout mice when the miR-103-mimic was administered to their arcuate nucleus (*12*). miRNAs are also chief regulators of the various stages involved in adult neurogenesis from the subventricular zone of the lateral ventricle and the subgranular zone of the hippocampus (*13*, *14*).

Collectively, all these studies suggest that miRNAs are potent regulators of adult neurogenesis in response to external stimuli, as well as regulators of body weight in response to dietary changes. Thus, they are a vital link to understand the mechanisms of neural circuit modifications by HFD-mediated tanycytic neurogenesis (*13*, *15*–*19*).

In this study, we have analyzed the miRNA profile of $BrdU^+$, neurogenic β2-tanycytes in the hypothalamus of female C57BL/6j mice after subjecting them to an acute HFD feeding paradigm. Further, using a combination of network analysis and cell fate mapping, we have identified the miRNA-dependent molecular framework underpinning β2-tanycytic neurogenesis and the functional activity of newborn neurons following HFD feeding.

Results

Identification of diet-regulated miRNAs from neurogenic tanycytes

To identify diet-regulated miRNAs from neurogenic tanycytes present in median eminence, female mice were fed with HFD during P45 – P75 and tanycytes undergoing neurogenesis were labelled by BrdU incorporation (Fig 1A and S1). These $BrdU^+$ tanycytes (Fig 1B and Fig S1) were laser captured from the median eminence and differential expression of miRNAs were analysed by miRNA arrays. We observed that 32 miRNAs were differentially expressed upon HFD feeding, whereas 5 miRNAs were differentially expressed in NCD fed mice. Among these transcripts, a cohort of miRNAs; miR-382 (log_2FC = 11.394, FDR = 0.021), miR-145 (log_2FC = 7.219, FDR = 0.0244), miR-196 (log_2FC = 6.744, FDR = 0.0123), miR-1894 (log_2FC = 11.023, FDR = 0.0297) and let-7b (log_2FC = 6.680, FDR = 0.0258) were significantly up-regulated upon HFD feeding (Fig 2B). Whereas NCD feeding significantly enhanced the expressions of let-7d (log_2FC = 5.227, FDR = 0.0072), let-7i (log_2FC = 3.932, FDR = 0.0349) and let-7e (log_2FC = 3.275, FDR = 0.049) (Fig 1C).

A.

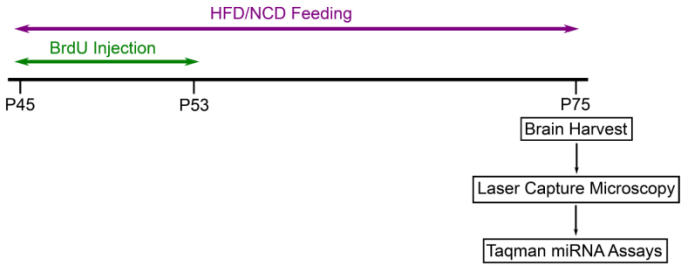

B.

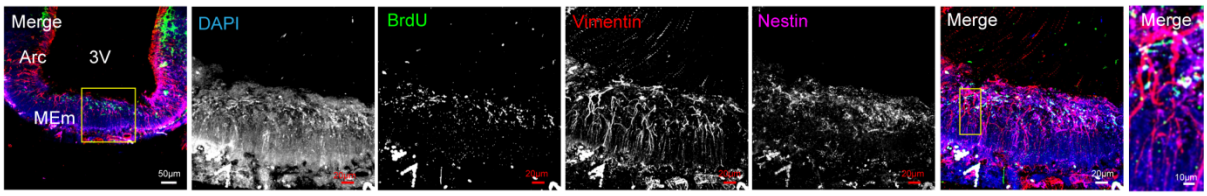

C.

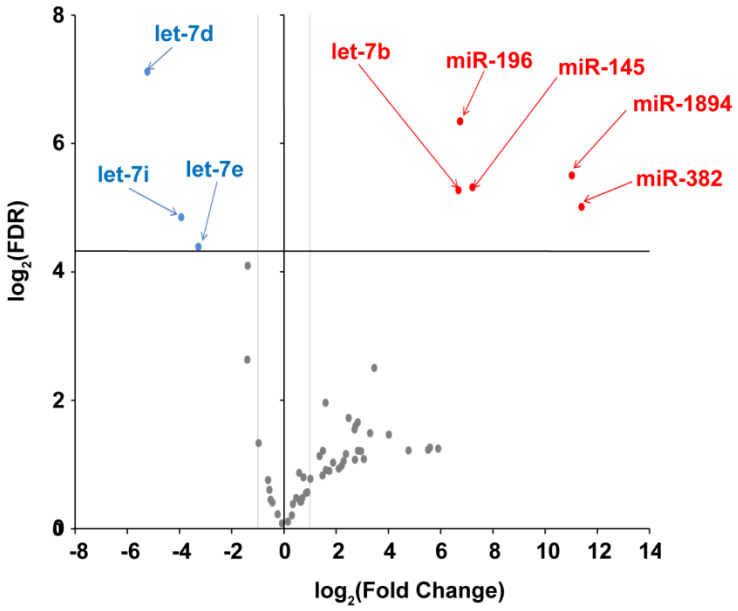

Figure 1: Differentially expressed miRNAs identified from adult neurogenic tanycytes in median eminence.

(A) Paradigm showing identification of miRNAs upon HFD/NCD. (B) Photomicrograph showing BrdU labelling of Vimentin^{+} β2 tanycytes in median eminence (MEm). (C) Volcano plot showing upregulated miRNAs following HFD (red) or NCD (blue) feeding. Significant change in miRNA expression (marked by arrow). N = 3 independent experiments. Two-tailed t-test was performed and post hoc false discovery rates (FDR) was analyzed using the Benjamini-Hochberg method. Arc: Arcuate Nucleus, 3V: Third ventricle.

In silico identification of diet-regulated miRNA targets:

To determine the mechanism of miRNA-mediated control of adult hypothalamic neurogenesis, the mRNA targets of the HFD-responsive miRNAs; miR-1894, miR-382, miR-145, miR-196 and let-7b, were analyzed. The putative targets containing binding sites for all five miRNAs were obtained from the TargetScan, miRdb and PicTar databases. We have selected 1204 transcripts represented in all three databases.

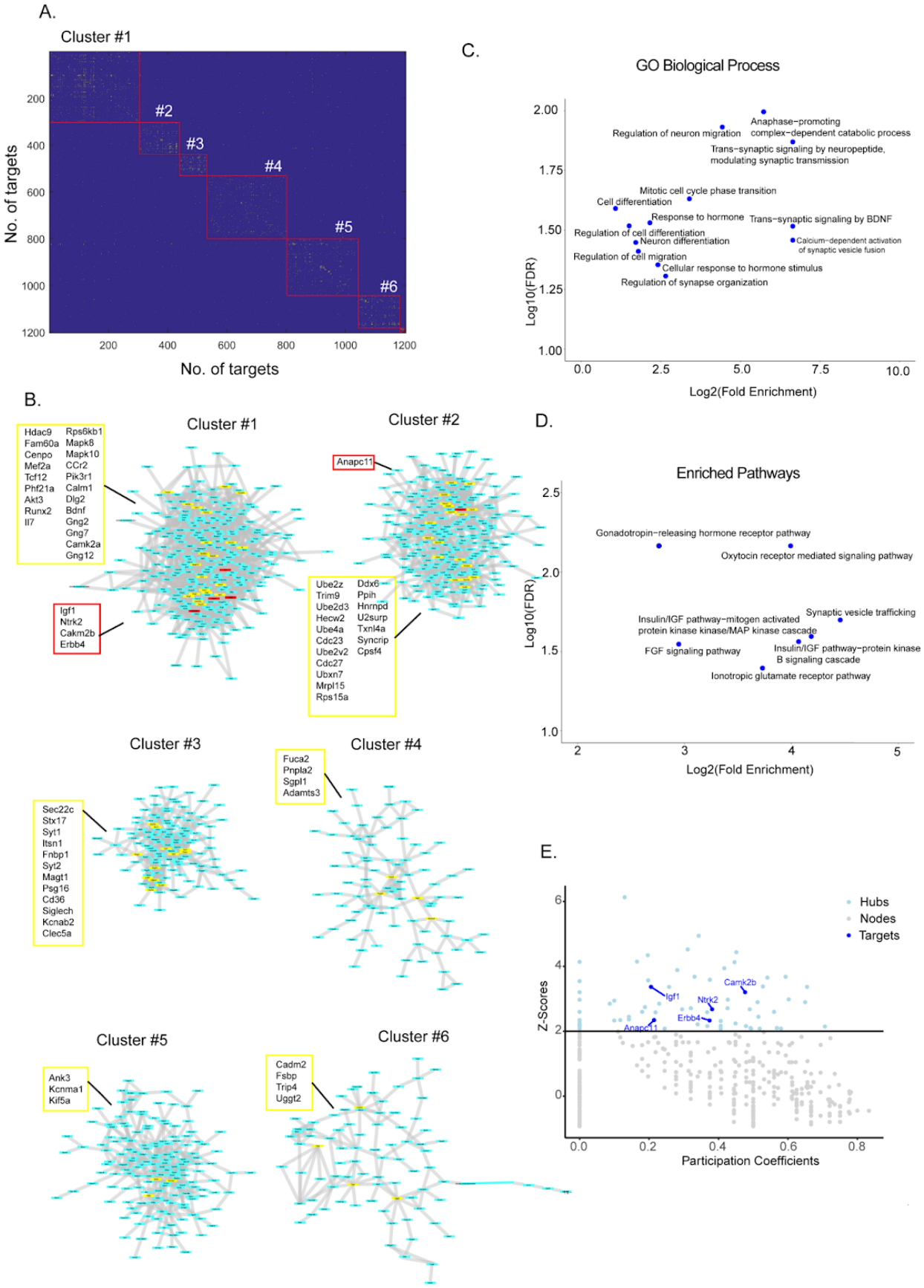
A.
Cluster #1
#2
#3
#4
#5
#6
No. of targets
No. of targets
B.
Cluster #1
Hdac9 Rps6kb1
Fam60a Mapk8
Cenpo Mapk10
Mef2a CCr2
Tcf12 Pik3r1
Phf21a Calm1
Akt3 Dlg2
Runx2 Bdnf
Il7 Gng2
Gng7
Camk2a
Gng12
Igf1
Ntrk2
Cakm2b
Erbb4
Cluster #2
Anapc11
Ube2z Ddx6
Trim9 Ppih
Ube2d3 Hnrnpd
Hecw2 U2surp
Ube4a Txnl4a
Cdc23 Syncrip
Ube2v2 Cpsf4
Cdc27
Ubxn7
Mrpl15
Rps15a
Cluster #3
Sec22c
Stx17
Syt1
Itsn1
Fnbp1
Syt2
Magt1
Psg16
Cd36
Siglech
Kcnab2
Clec5a
Cluster #4
Fuca2
Pnpla2
Sgpl1
Adamts3
Cluster #5
Ank3
Kcnma1
Kif5a
Cluster #6
Cadm2
Fsbp
Trip4
Uggt2
C.
GO Biological Process
Anaphase−promoting complex−dependent catabolic process
Regulation of neuron migration
Trans−synaptic signaling by neuropeptide, modulating synaptic transmission
Mitotic cell cycle phase transition
Cell differentiation
Response to hormone
Trans−synaptic signaling by BDNF
Regulation of cell differentiation
Neuron differentiation
Calcium−dependent activation of synaptic vesicle fusion
Regulation of cell migration
Cellular response to hormone stimulus
Regulation of synapse organization
Log10(FDR)
Log2(Fold Enrichment)
D.
Enriched Pathways
Gonadotropin−releasing hormone receptor pathway
Oxytocin receptor mediated signaling pathway
Synaptic vesicle trafficking
Insulin/IGF pathway−mitogen activated protein kinase kinase/MAP kinase cascade
FGF signaling pathway
Insulin/IGF pathway−protein kinase B signaling cascade
Ionotropic glutamate receptor pathway
Log10(FDR)
Log2(Fold Enrichment)
E.
Hubs
Nodes
Targets
Camk2b
Igf1
Ntrk2
Erbb4
Anapc11
Z-Scores
Participation Coefficients

Figure 2: *In silico* network analysis of target transcripts containing binding sites of HFD-regulated miRNAs.

(A) Adjacency matrix showing community clustering (red boxes) based on the interaction between each target as a node. (B). 6 clusters of the network of target transcripts containing binding sites for all five miRNAs. All hubs are indicated in the "yellow" box. Hubs selected for target validation via reporter assay are represented in the "red" box. (C) Scatter plots showing fold enrichment of significant GO-terms in Biological Process. (D) Scatter plots showing fold enrichment of significant GO-terms from pathway analysis. (E) Scatter plot showing the z-scores and the participation coefficients for all nodes in the network. Nodes are considered "hubs" for z-score > 2. Hubs selected for reporter analysis are indicated.

Since, protein-protein interactions influence the miRNA-dependent cellular functions, we have analyzed the interactions between all 1204 putative targets using the StringDB database. Graph theory based network analysis was performed to determine the key miRNA target transcripts. Nodes (mRNA targets) were clustered using Louvain's community clustering method (*20*). Stable optimization of the clustering of the nodes using the above method was achieved using a resolution parameter ranging from 0.5 – 0.75 (Fig 2A). We observed a highly modular network among the targets of the upregulated miRNAs upon HFD feeding, whereas this modularity is absent upon NCD feeding. We have detected 11 modules in the HFD network, out of which 6 modules are highlighted (Fig 2B). Hence, this network modularity is a key target selection criterion for further analysis as clustered transcripts within a network could potentially drive neurogenesis in the tanycytes upon HFD feeding.

Among the modularized community clusters, inter-community and intra-community measures of nodal activity were analyzed to determine the important target nodes that are critical for the entire network. Participation coefficient, a marker for inter-community interactions, was analyzed for all nodes to define the hubs. We have analyzed z-scores, a marker for intra-community interactions, to select the critical hubs in the network. Hubs with z-scores > 2 were selected for Gene Ontology (GO) analysis. We reasoned that these hubs contain key transcripts that can regulate multiple nodes. We observed that significantly enriched GO-terms included neuron differentiation (Fold Enrichment = 3.28; FDR = 0.0357), mitotic cell cycle phase transition (Fold Enrichment = 10.55; FDR = 0.0234), cellular response to hormone stimulus (Fold Enrichment = 5.32; FDR = 0.0443), trans-synaptic signaling by BDNF (Fold Enrichment = 100; FDR = 0.0247), trans-synaptic signaling by neuropeptide modulating synaptic transmission (Fold Enrichment = 100; FDR = 0.0135), regulation of cell migration (Fold Enrichment = 3.47; FDR = 0.0389) and anaphase-promoting complex-dependent catabolic process (Fold Enrichment = 53.1; FDR = 0.0101) (Fig 2C). We have also assessed significant GO-enriched pathways that includes insulin/IGF pathway-protein kinase B signaling cascade (Fold Enrichment = 16.77; FDR = 0.0274), insulin/IGF pathway-mitogen activated protein kinase cascade (Fold Enrichment = 18.21; FDR = 0.0254), ionotropic glutamate receptor pathway (Fold Enrichment = 13.27; FDR = 0.0402), FGF-signaling pathway (Fold Enrichment = 7.71; FDR = 0.0284) and gonadotropin-releasing hormone receptor pathway (Fold Enrichment = 6.78; FDR = 0.00683) (Fig 2D).

Based on the GO-enrichment analysis, we have selected IGF1 (Participation Coefficient = 0.2058, z-Score = 3.3689), NTRK2 (Participation Coefficient = 0.3816, z-Score = 2.6779), CAMK2B (Participation Coefficient = 0.4764, z-Score = 3.2045), ERBB4 (Participation Coefficient = 0.3743, z-Score = 2.3324) and ANAPC11 (Participation Coefficient = 0.2145, z-Score = 2.3458) for further validation using a reporter assay (Fig 2E).

Verification of miRNA-mRNA interactions *in vitro*.

We have used luciferase reporter assay following inhibition of HFD-regulated all five miRNAs activity to validate the miRNA-mRNA interactions for the selected hub transcripts identified by our *in silico* analysis. To sequester all five miRNA activity together, a sponge construct was cloned into a vector that co-expressed tdTomato (Fig 3A). We analyzed the efficacy of the miRNA sponge construct by the fluorescence intensity of tdTomato expression.

A. Sponge Construct Design:

B. Luciferase Construct Design:

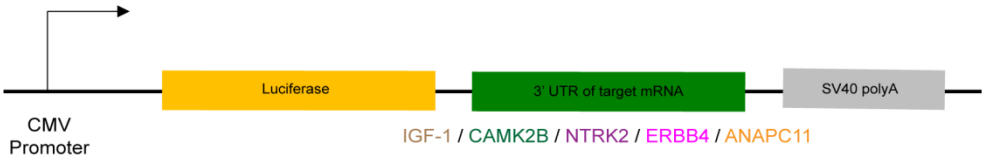

C.

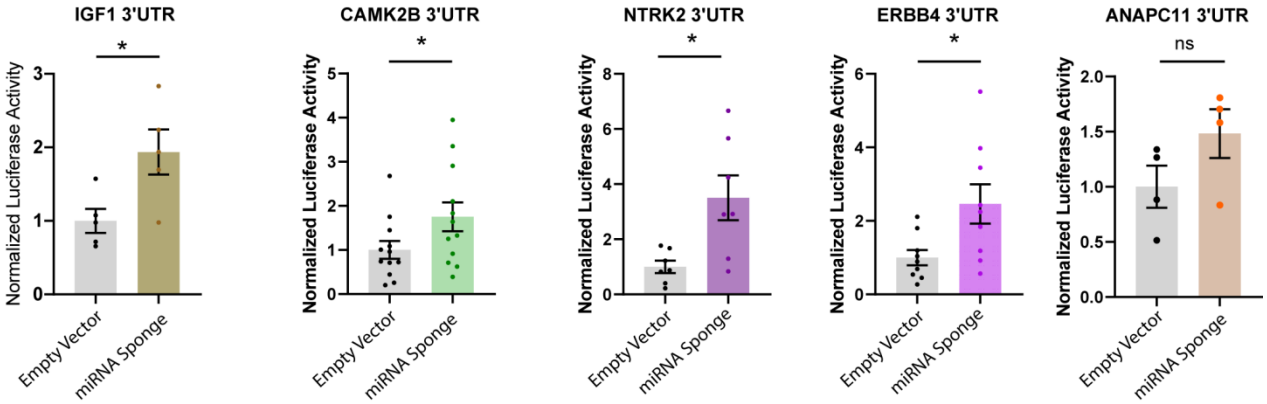

Figure 3: *In vitro* validation of mRNA target interactions with HFD responsive miRNAs.

(A) Schematic design of miRNA sponge construct. (B) Schematic design of luciferase reporter. (C) Quantitation of luciferase reporter expression driven by 3'UTRs of IGF1, NTRK2, CAMK2B, ERBB4 and ANAPC11 following simultaneous inhibition of all 5 HFD-regulated miRNAs' activity. N = 4 – 11 independent experiments. *$p < 0.05$. Data shown as mean ± SEM. Two tailed t-test with Welch's correction.

Administration of the miRNA sponge significantly reduced the intensity of tdTomato expression (65.05% ± 12.52% decrease, $p<0.0001$) (Fig. S2B-C) as compared to the tdTomato expression in the control vector. The 3'UTRs of each transcript containing the binding sites of all five miRNAs were fused to Gaussia luciferase reporter (Fig 3B). We co-transfected the miRNA sponge and each of the reporters into Neuro-2a cells. The reporter activity was normalized to the activity of the constitutively expressed Renilla luciferase. We observed that simultaneous inhibition of all five miRNAs up-regulated by HFD led to the significant enhancement of reporter activity driven by 3'UTRs of IGF1 (0.9368 ± 0.3469 fold increase, $p = 0.0349$), NTRK2 (2.504 ± 0.8448 fold increase, $p = 0.0213$), CAMK2B (1.211 ± 0.4275 fold increase, $p = 0.0137$) and ERBB4 (1.461 ± 0.5733 fold increase, $p = 0.0282$) (Fig 3C). However, we did not detect any significant change in reporter activity driven by 3'UTR of ANAPC11 (0.4821 ± 0.2916 fold increase, $p = 0.1504$) (Fig 3C).

HFD-induced miRNAs regulate functional integration of nascent neurons into the hypothalamic feeding circuit.

A.

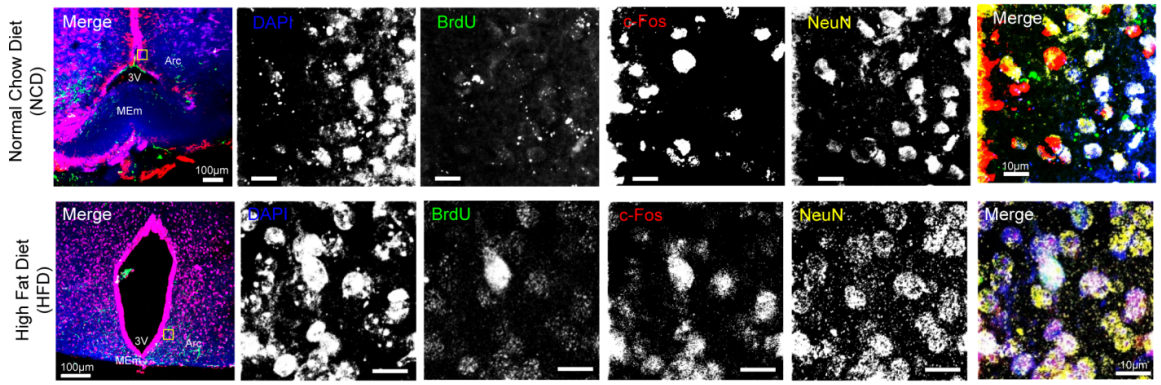

B.

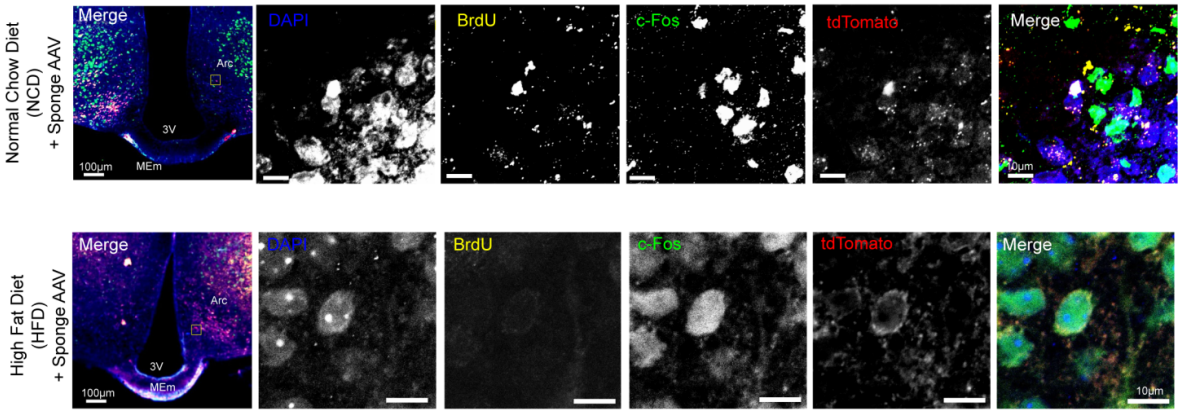

C.

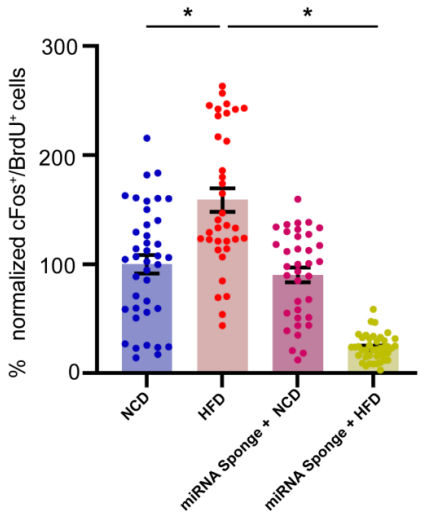

Figure 4: HFD-induced miRNAs regulate functional integration of newborn neurons into the feeding circuit.

(A) Photomicrograph showing functional integration of diet-regulated nascent neurons. Low magnification image of the brain section showing all channels [DAPI (blue), BrdU (green), c-Fos (red), NeuN (yellow)] within the merged (white) image. High magnification images of brain sections labelled with DAPI (blue), BrdU (green), c-Fos (red), NeuN (yellow) and merged (white) in HFD or NCD fed brains. Scale bars are indicated. (B) Photomicrograph showing functional integration of diet-regulated nascent neurons following inhibition of miRNAs activity. Low magnification image of the brain section showing all channels [DAPI (blue), c-fos (green), tdTomato (red), NeuN (yellow)] represented in a merged (white) image. High magnification images of brain sections labelled with DAPI (blue), c-Fos (green), tdTomato (red), NeuN (yellow) and merged (white) in HFD or NCD fed brains. Scale bars are indicated. (C) Quantitation of $BrdU^+$ and c-Fos^+ neurons. Data is shown as mean ± SEM. N = 35-42 brain section from 3 independent experiments. *$p < 0.0001$. One-way ANOVA with Fisher's LSD test.

To study the functional integration of newborn neurons into the feeding circuit of hypothalamus, we have analyzed c-Fos expression in $BrdU^+$ neurons as an indicator of neuronal activity. We have also quantified the number of $BrdU^+$ and c-Fos^+ neurons in the arcuate nucleus (ARC) following HFD feeding with or without inhibition of all 5 miRNAs activity together by miRNA sponge. We have observed a significant increase in $BrdU^+$ and c-Fos^+ neurons upon HFD feeding (58.84% ± 10.58% increase, $p<0.0001$) (Fig 4A and 4C) as compared to mice fed with NCD. Furthermore, the sequestration of HFD-regulated miRNAs activity significantly reduced the number of $BrdU^+$ and c-Fos^+ neurons as compared to HFD-fed mice with intact miRNA function (66.91% ± 10.39% decrease, $p<0.0001$) (Fig 4B and 4C). Our data demonstrates that HFD-induced miRNAs play a key role in functional integration of nascent neurons in adult hypothalamus.

HFD-induced nascent neurons in adult hypothalamus differentiate into functionally active orexigenic neurons in the feeding circuit.

To determine the cell fate of adult born $BrdU^+$ nascent neurons upon HFD feeding, we have analyzed whether these neurons differentiate into POMC-expressing anorexigenic or AgRP-expressing orexigenic neurons. These two neuronal types are key determinants of feeding circuit function. Brain sections following HFD/NCD feeding and BrdU labelling were analyzed for co-expression of POMC or AgRP and neuronal nuclear marker, NeuN. We have observed that HFD fed mice showed a significant enhancement of AgRP expressing $BrdU^+$ neurons (59.59% ± 19.88% increase, $p = 0.004$) as compared to mice fed with NCD (Fig 5A and Fig 5C).

To determine whether orexigenic neurons are functionally active, we have assessed the expression c-Fos in AgRP expressing neurons in the arcuate nucleus upon HFD feeding. We observed that the orexigenic neurons were indeed functionally active as detected by significant enhancement of c-Fos expressing AgRP neurons (41.91% ± 3.80% increase, $p < 0.0001$) (Fig 5B and Fig 5D) from HFD fed mice as compared to mice fed with NCD. Although, we have detected a similar enhancement of POMC expressing $BrdU^+$ neurons (83.35% ± 27.33% increase, $p = 0.004$) in HFD-fed mice (Fig S3) but they are not

functionally active in the arcuate nucleus (Fig S3). Taken together, our data suggests that HFD feeding leads to production of functionally active orexigenic neurons in the adult hypothalamus.

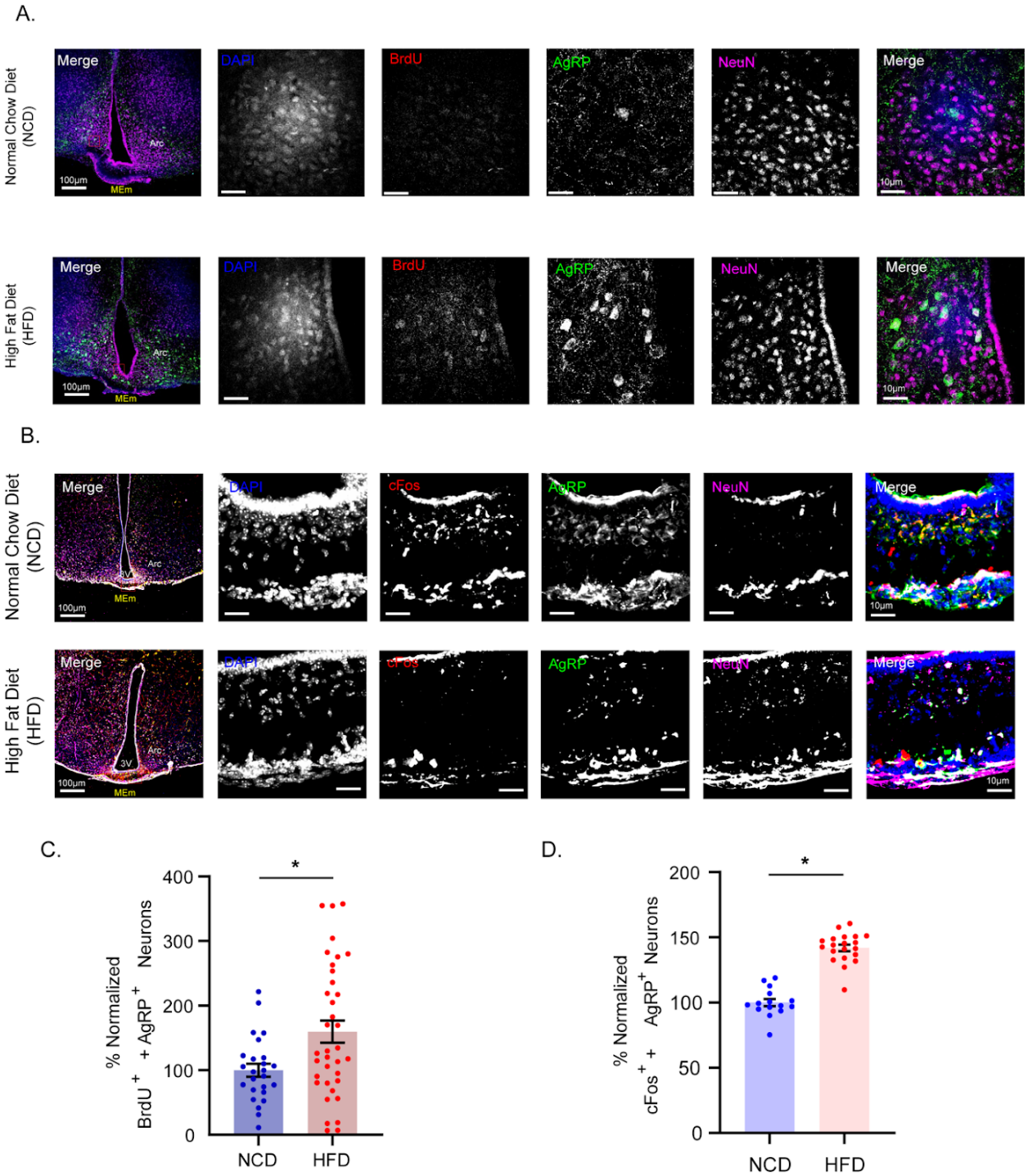

Figure 5: Diet-induced differentiation of nascent neurons into functionally active AgRP neurons.

(A) Photomicrographs represent orexigenic fate of diet-induced nascent neurons upon HFD or NCD feeding. Low magnification image of brain sections of all channels [DAPI (blue), BrdU (red), AgRP (green), NeuN (magenta)] were merged (white). High magnification images of brain sections labelled with DAPI (blue), BrdU (red), AgRP (green), NeuN (magenta) and merged (white). Scale bars are indicated. (B) Photomicrographs showing functionally active AgRP neurons upon HFD or NCD feeding. Low magnification image of brain sections of all channels [DAPI (blue), c-Fos (red), AgRP (green), NeuN (magenta)] were merged (white). High magnification images of brain sections labelled with DAPI (blue), c-Fos (red), AgRP (green), NeuN (magenta) and merged (white). Scale bars are indicated. (C) Quantitation of normalized $BrdU^+$ and $AgRP^+$ neurons. Data is shown as mean ± SEM. N = 25-36 brain sections from 3 independent experiments. Two-tailed t-test with Welch's correction. (D) Quantitation of normalized $c\text{-}Fos^+$ and $AgRP^+$ neurons. Scale bars are indicated. Data shown as mean ± SEM. N = 15-20 brain sections from 3 independent experiments. Two-tailed t-test with Welch's correction.

Discussion:

The research on adult neurogenesis has extended beyond the classical regions of the subventricular zone and the subgranular zone to include the roles of other neurogenic niches in the adult mouse brain (*6*, *21*, *22*). The interests in the neurogenic niches of the hypothalamus and its response to the dietary factors and subsequent behavioral and metabolic modifications of the physiological state have grown recently with many studies stressing upon their importance (*1*, *2*, *23*).

One such unique neurogenic niche is presented by tanycytes, a specialized form of radial-glia like ependymal cells bordering the third ventricle and found in the median eminence and the arcuate nucleus of the hypothalamus. Tanycytes are regulated by a plethora of factors including diet, hormones, gender and age, leading to multiple patterns of neurogenesis in the hypothalamus (*6*). Based on their morphological and molecular characteristics, tanycytes are classified as α1, α2 or β1, β2 tanycytes (*24*). Of particular interest are the β2 tanycytes found lining the median eminence in female mice; neurogenesis is found to occur from these specialized cells in response to HFD in young adult female mice, directly resulting in body weight gain (*2*). The physiological impact of this neurogenesis has been studied with its ablation, but the mechanism of neural circuit modifications and the underlying molecular factors are not understood.

In this study, we have studied the molecular mechanisms regulating the β2- tanycytic neurogenesis induced by HFD feeding in young adult female mice. We have identified the crucial roles of a combination of miRNAs in the induction of neurogenesis in the tanycytes and their subsequent functional integration into the feeding circuitry in the arcuate nucleus (Fig.1) The identification of a cohort of miRNAs and their interacting targets in regulating the neurogenesis is novel, as previous studies (*25*–*27*) have merely

focused on identifying the singular expression patterns of miRNAs and the large number of mRNAs that they target. The detection of the five HFD-induced miRNAs is novel as they are expressed from diverse genomic loci, and do not adhere to a single family or cluster of miRNAs (*28*). Although this kind of approach resulted in the understanding of the individual roles of miRNAs in the regulation of HFD-induced obesity; what remained elusive to our comprehension was a holistic perspective of how diet-influenced miRNAs caused a major change in the existing translatome that led to neurogenesis, and how the functional integration of these nascent neurons occurred within the existing neural circuitry.

Our study resolved this void by employing a network theory-based miRNA target analysis and assessed functions of these target transcripts using GO analysis. We have selected transcripts containing binding sites for all five HFD-induced miRNAs as detected by all three major target prediction algorithms. The network analysis segregated transcripts into specific clusters based on the interactions between each participating transcripts within the cluster. Clusters were selected based on high intra-community interactions between transcripts or “nodes” of the network and some of these nodes functioning as “hubs” to influence the activity of many “nodes”. We have selected hubs based on Z-score analysis and analyzed their GO-enrichment and GO-pathways to predict their function linked with neurogenesis, neuronal migration and neuronal differentiation. For example; GO terms such as “response to hormone”, “neuron differentiation”, “regulation of cell migration” and “Calcium-dependent activation of synaptic vesicle fusion”; and GO pathways like “insulin/IGF pathway-MAP kinase cascade”, “insulin/IGF pathway-PKB signaling cascade”, “FGF signaling pathway”; were enriched. The enrichment of these pathways and gene ontologies reveal the existence of a neurogenic network regulated by the cohort of all five miRNAs induced by HFD feeding. This network is highly modularized and is specific to the functions of neurogenesis in the β2 tanycytes when mice were fed with HFD. This specificity towards the neurogenic profile is absent in the network formed by the targets of NCD-enriched miRNAs. Thus, the interactions of the mRNA targets by the cohort of HFD-responsive miRNAs could induce neurogenesis in response to HFD, and thereby modulate the underlying feeding circuitry.

Among the hubs in the network, we have focused on the important regulators of cellular function and neurogenesis, such as IGF1, NTRK2, CAMK2B, ERBB4 and ANAPC11. The above transcripts are highly characterized in their role in neurogenesis and physiological energy homeostasis. IGF1 is a neurotrophic factor that plays a significant role in neurogenesis, neuronal differentiation and neuronal survival (*29*–*31*), and an important effectuator of cell division (*32*). Exercising and similar activities have been known to increase IGF1 expression leading to neurogenesis (*29*). NTRK2 is a well-characterized receptor of BDNF, which plays major roles in neural survival and metabolic disorders (*33*). Mutations in NTRK2 have been linked to obesity resulting from hyperphagia (*33*–*36*).

CAMK2B is a calcium dependent kinase that is necessary for dendritogenesis and synaptogenesis (*37*). ERBB4 is a receptor tyrosine kinase which binds to growth factors such as neuregulins which promote the formation of functional synapses (*38*, *39*). Thus, our *in silico* graphical network analysis, identified the interactions of all common putative targets of the miRNAs and determined the relevance of the targets as central effectors of this miRNA induced β2- tanycytic neurogenesis (Fig. 2).

In order to validate the importance of miRNA targets highlighted in our network analysis, a miRNA sponge was designed in addition to luciferase reporter constructs (Figure 3). The miRNA sponge is a combinatorial sponge sequence that contains six binding sites to each of the five miRNAs arranged in tandem (Fig.3A). Applications of such miRNA-sponges result in the identification of possible translational fates of miRNA targets occurring due to the simultaneous inhibition of all five miRNAs, providing a newer perspective than previous studies which only focused on elucidating the physiological role of individual miRNAs. The mRNAs controlled by the HFD-induced miRNAs are diverse in their molecular characteristics and functions; therefore, effectuating a robust and concomitant change in the translation of all these mRNAs is more relevant physiologically.

We used luciferase reporter constructs harboring the entire 3' UTR of each of the selected mRNA hubs; IGF1, NTRK2, CAMK2B, ERBB4 and ANAPC1 to validate their direct regulation by the HFD-induced miRNAs (Figure 3B-3C). Of note, the above mRNAs are central hubs to the entire neurogenic network in HFD-fed mice; therefore, changes to the translational profile of these mRNAs due to the combinatorial inhibition of all five miRNAs results in more widespread modification of a plethora of diverse molecular cascades relevant to neurogenesis, that finally lead to modifications of the feeding circuitry.

We further investigated the functional role of HFD-induced miRNAs in promoting β2-tanycytic neurogenesis (Fig. 4). Modification of a neuronal circuitry may be achieved by the functional integration of newborn neurons into the preexisting neural connectivity; such neurons exhibit c-Fos expression (*40*). Since HFD feeding in young adult female mice specifically leads to β2- tanycytic neurogenesis in the median eminence (Figure 1B) (*6*); $BrdU^+$ neurons would effectively indicate nascent neurons of tanycytic origin. To identify whether these newborn neurons from β2- tanycytes are functionally active in the arcuate nucleus and median eminence of the hypothalamus, we looked at their c-Fos expression levels by immunostaining. HFD-fed female mice possessed a higher percentage of functionally active, nascent neurons compared to mice fed with NCD; these $BrdU^+$ $c\text{-}Fos^+$ neurons in HFD-fed mice were lost upon the inhibition of miRNA activity *in vivo* by miRNA sponge (Fig 4A-4C). Since no other variable was different between HFD-fed and NCD-fed mice barring their diet, the additional expression of $c\text{-}Fos^+$ and $BrdU^+$ neurons observed in the former may be attributed to HFD alone.

Although, previous studies (*2*, *5*) have investigated the outcomes of tanycytic neurogenesis by performing complete ablation of the tanycytic population by X-ray irradiation; this method is unable to address specific molecular functions of the tanycytes as they are completely abolished in the median eminence. Here, *in vivo* application of miRNA-sponges circumvents such global abrogation of tanycytes, and highlights the role of specific miRNAs in fine-tuning the translational landscape of the β2-tanycytic neurogenic niche at a molecular resolution.

Furthermore, the same studies identified the connection between the abrogation of the tanycytic population and abolition of HFD-mediated weight gain. Shifts in the metabolic state of HFD-fed mice are a manifestation of sustained changes to the feeding circuitry; the causality of which has not been explored in any study to date. Therefore, we proceeded to identify the neuronal fate of the nascent β2-tanycytic neurons in the feeding circuitry (Fig 5) in response to acute HFD feeding. We observed a preferential tendency of $BrdU^+$ tanycytic neurons to differentiate into functionally active orexigenic $AgRP^+$ neurons. AgRP neurons induce Hyperphagia (*9*) and energy storage as fat in mice (*2*). Thus, our observations establish the causal link between HFD-induced tanycytic neurogenesis and weight gain in female mice. Acute HFD feeding leads to enhanced β2-tanycytic neurogenesis and the preferential differentiation of these functionally active (c-Fos^+) neurons into $AgRP^+$ orexigenic neurons; thereby shifting the effective behavioural output of the neural circuitry towards hyperphagic obesity.

Of note, acute HFD feeding also resulted in the increased differentiation of β2-tanycytes into $POMC^+$ anorexigenic neurons. However, there was no difference in the functional integration of anorexigenic neurons in HFD-fed mice *vs* NCD-fed mice. We postulate that β2-tanycytic neurogenic differentiation into $POMC^+$ cell fate could act as a “brake” to HFD-induced metabolic changes. But, the acute feeding paradigm of HFD is unable to induce the functional integration of anorexigenic neurons, thereby showing a preference towards orexigenic neuron-mediated hyperphagia and weight gain. This lack of functional integration of the nascent POMC neurons is of future interest as they could possibly be a link in contending against the deleterious effects of HFD feeding. Although tanycytic neurogenesis of the median eminence is induced by HFD in the young adult female mice, observations on further changes in the molecular profiles of tanycytic neurons in older animals is beyond the scope of this study. Future investigations on age-dependent and sex-dependent discrepancies in the molecular identities of HFD-induced neurons may provide useful insights towards combating metabolic disorders such as obesity and hyperphagia.

Materials and Methods

Stereotaxic Surgery:

Female C57BL6/j animals at P21 - P25 were used for the experiments. Cannulas were prepared from a 23G needle, modified for the appropriate ventral depth to be placed atop the skull as described in (*41*). They were fitted with a dummy copper wire inside to prevent the leak of CSF or the entry of external irritants into the lateral ventricle. This cannula structure was then sterilized before the surgeries.

Animals were anaesthetized with Ketamine (80mg per 1 kg of body weight) and Xylazine (20mg per 1kg of body weight) administered via subcutaneous injections. Post anesthesia, the hairs were trimmed and the animals were affixed onto the stereotactic instrument. The skull was exposed and the coordinates of the Bregma was determined. A hole for the cannula was drilled at the stereotaxic coordinates (Anterior +0.02cm; Lateral -0.08cm; Ventral -0.25cm w.r.t Bregma). Stereotaxic coordinates were obtained from the Mouse Coronal Atlas from the Allen Brain Atlas (mouse.brain-map.org). The cannula was lowered at the previously drilled site. Post the implant of the cannula, a small hole was drilled on the skull posterior to the cannula. A small screw was screwed onto the skull. Then, the skull was covered up with the dental cements and the quick polymer. Then, the animals were allowed to recover from surgeries for 10-12 days, with regular changing of the sterile dummy copper wire inside the cannula.

Animal experiments were performed with the approval of the Institutional Animal Ethics (IAEC) committee of National Brain Research Centre.

Feeding and Intracerebroventricular/Intraperitoneal injections of BrdU:

Animals were either started on a Rodent Diet with 60 kcal% fat diet (Research Diets, Inc. (RD #12492)) [HFD], or continued with the normal chow diet [NCD] at P45, and this was continued till they turned P75, when the animals were sacrificed for further experiments. Animals were given *ad libitum* access to the diet and water. All the animals used for miRNA expression analysis via Taqman Arrays, were implanted with cannulas (n=3 animals for n=1 experiment for 3 experiments). These animals were injected with BrdU intracerebroventricularly at 2 injections a day of 10 µgms each from P45-P53. None of the animals used for immunostaining experiments were implanted with cannulas (n=1 animal for n=1 experiment for 3 experiments). These animals were injected with 10mg of BrdU per kg body weight intraperitoneally of the respective animals twice a day from P45-P53.

Immunostaining:

Animals were anaesthetized and perfused transcardially at P75 with 1X PBS / 4% Paraformaldehyde. The brains were then isolated and stored in PFA and processed with 30% Sucrose for cryosectioning. Brains were sectioned at 40 µm thickness and collected onto gelatin-coated slides for processing. Sections were then introduced to a HCl-Borate Buffer method for breaking the chromosomes and hybridized with anti-BrdU antibodies. They were also co-stained with anti-Vimentin, anti-Nestin, anti-POMC, anti-AgRP, anti-c-Fos and anti-NeuN antibodies as per the requirement of the different studies.

Laser Capture Microscopy:

Animals were sacrificed on P75, and the brains were flash frozen in liquid N_2. Brains were sectioned at 12 µm thickness, and carried onto MembraneSlide 1.0 PEN. Sections were fixed with PFA, then stained for BrdU in RNase-free solutions, and conjugated with fluorescent tags to visualize under the microscope. Zeiss PALM MicroBeam Laser Microdissection microscope was used to visualize the fluorescent tags of Brdu, and they were microdissected, collected onto miRNA lysis buffers and pooled for miRNA isolation using the Mirvana Total RNA isolation protocol (Applied Biosystems).

TaqMan Low Density Array:

The RNA from the captured neurogenic population was reverse transcribed using the Megaplex™ RT Primers, Rodent Pools Set v3.0. Then, the cDNA was amplified using Megaplex™ PreAmp Primers, Rodent Pool Set v3.0. The amplified cDNA was then used to analyze the miRNA expressions determined using TaqMan™ Array Rodent MicroRNA A+B Cards Set v3.0. Data was then collected from 3 experiments, and average expression of the miRNAs were analyzed and plotted.

miRNA target identification:

Annotated and putative targets of diet responsive miRNAs were obtained from the databases of TargetScan (*42*), miRdb (*43*, *44*) and PicTar (*45*). Common identified targets for each miRNA across all the databases were acquired. Then, the common targets for the cohort of all diet responsive miRNAs were also pooled into a single list of 1204 targets.

Network Analysis:

Interactions between the common targets of the HFD-enriched miRNAs were determined using the String database (https://string-db.org/). The interaction network of the targets was then analyzed in Matlab using Brain Connectivity Toolbox (*20*). All mRNA targets of the miRNAs were assigned as nodes of the network and the interactions between two

nodes were considered as the edges of the network. Community analysis was performed using Louvain's method to determine the community clusters of the nodes. Within module z-scores and participation coefficients were determined for each node and plotted. Nodes were determined to be hubs if their corresponding z-scores were > 2.

Gene Ontology Analysis:

Hubs selected by z-score analysis were used for the analysis of Gene Ontologies using PANTHER Database (http://pantherdb.org/) (doi:10.5281/zenodo.6399963). GO Enrichment for the hubs was obtained from the database. Fisher's exact test was performed to test the significant enrichment of the transcripts in annotated datasets such as, GO: Biological Process and Panther Pathways, and the FDR values were generated using Panther statistical overrepresentation test. Significantly enriched GO terms were analyzed and plotted.

miRNA sponge construct design:

Bulged binding sites against the seed sequences of HFD enriched miRNAs (from miRBase (*28*)) were designed and synthesized (*46*) 6 sites for each of the 5 miRNAs (miRs -382, -145, -196, -1894 and let-7b) were included in the synthesized construct (*47*). This construct was then incorporated into the ORF of the fluorescent marker tdTomato. An empty vector did not express the sponge sites. The plasmids were transfected into Neuro-2a cells for luciferase assays, and they were packaged into AAVs for injection into the hypothalamus for imaging. The designed sponge sequence is shown below with the bulged binding sites for miR-382 (red), miR-145 (blue), miR-196 (green), miR-1894 (magenta) and let-7b (orange) are highlighted in the sequences.

miRNA Sponge Fwd

(5'–3')
AATTCAAAAAGTGCCACCGTGAATGATTATAAAAAGTGCCACCGTGAATGATTATAA
AAAGTGCCACCGTGAATGATTATAAAAAGTGCCACCGTGAATGATTATAAAAAGTG
CCACCGTGAATGATTATAAAAAGTGCCACCGTGAATGATTATCAAGAACATGCTTC
CAGGAATTTATCAAGAACATGCTTCCAGGAATTTATCAAGAACATGCTTCCAGGAAT
TTATCAAGAACATGCTTCCAGGAATTTATCAAGAACATGCTTCCAGGAATTTATCAA
GAACATGCTTCCAGGAATTTATATCAGGTGACCGATGTCGTTGTTATATCAGGTGA
CCGATGTCGTTGTTATATCAGGTGACCGATGTCGTTGTTATATCAGGTGACCGATG
TCGTTGTTATATCAGGTGACCGATGTCGTTGTTATATCAGGTGACCGATGTCGTTG
TTATCTCCCTTCGATTCTCCCTTGCTTATCTCCCTTCGATTCTCCCTTGCTTATCTCC
CTTCGATTCTCCCTTGCTTATCTCCCTTCGATTCTCCCTTGCTTATCTCCCTTCGATT
CTCCCTTGCTTATCTCCCTTCGATTCTCCCTTGCTTATGGGAAGGCGTGGGTTGTA
TAGTTATGGGAAGGCGTGGGTTGTATAGTTATGGGAAGGCGTGGGTTGTATAGTTA

TGGGAAGGCGTGGGTTGTATAGTTATGGGAAGGCGTGGGTTGTATAGTTATTTATG
GGAAGGCGTGGGTTGTATAGA

miRNA Sponge Rev

(5'–3')
TCTATACAACCCACGCCTTCCCATAAATAACTATACAACCCACGCCTTCCCATAACT
ATACAACCCACGCCTTCCCATAACTATACAACCCACGCCTTCCCATAACTATACAAC
CCACGCCTTCCCATAACTATACAACCCACGCCTTCCCATAAGCAAGGGAGAATCGA
AGGGAGATAAGCAAGGGAGAATCGAAGGGAGATAAGCAAGGGAGAATCGAAGGG
AGATAAGCAAGGGAGAATCGAAGGGAGATAAGCAAGGGAGAATCGAAGGGAGATA
AGCAAGGGAGAATCGAAGGGAGATAACAACGACATCGGTCACCTGATATAACAAC
GACATCGGTCACCTGATATAACAACGACATCGGTCACCTGATATAACAACGACATC
GGTCACCTGATATAACAACGACATCGGTCACCTGATATAACAACGACATCGGTCAC
CTGATATAAATTCCTGGAAGCATGTTCTTGATAAATTCCTGGAAGCATGTTCTTGAT
AAATTCCTGGAAGCATGTTCTTGATAAATTCCTGGAAGCATGTTCTTGATAAATTCC
TGGAAGCATGTTCTTGATAAATTCCTGGAAGCATGTTCTTGATAATCATTCACGGTG
GCACTTTTTATAATCATTCACGGTGGCACTTTTTATAATCATTCACGGTGGCACTTTT
TATAATCATTCACGGTGGCACTTTTTATAATCATTCACGGTGGCACTTTTTATAATCA
TTCACGGTGGCACTTTTTGAATT

Luciferase reporter construct design:

Primers to amplify the 3'UTR sequences of miRNA targets, IGF1, NTRK2, CAMK2B, ERBB4 and ANAPC11 were designed. They were amplified from mouse brain cDNA and were incorporated into the pMiR-Report vector into the 3'UTR of the luciferase reporter.

IGF1_F TTAAACAGTTAAGCTAGGAAGTGCAGGAAACAAGACC

IGF1_R ATCCTTTATTAAGCTCATCTTAGGCTCCAGGCTTTCG

NTRK2_F TTAAACAGTTAAGCTAGGCATCTCCCGTCTACCTG

NTRK2_R ATCCTTTATTAAGCTAGAGCGTCTCCTGTCTTTGTC

CAMK2B_F TTAAACAGTTAAGCTACGGCAAGTGGCAGAATGTAC

CAMK2B_R ATCCTTTATTAAGCTACCTGCATTGCCCAGAAGTC

ERBB4_F TTAAACAGTTAAGCTCGCCCTACAGACACCGGAATAC

ERBB4_R ATCCTTTATTAAGCTCCTTTCATGTAGACGTACCCAATCC

ANAPC11_F TTAAACAGTTAAGCTATGTGTCGCCAGGAGTGGAAG

ANAPC11_R ATCCTTTATTAAGCTAGTCTCCCAGAAGCACAAGTC

Luciferase reporter assays:

Neuro-2a cells were transduced with miRNA sponge, or empty plasmids at 16 hrs post plating. Transfected cells were incubated in high glucose DMEM media (Gibco) with 5% fetal bovine serum and maintained at 5% CO_2 and 37°C. Cells were simultaneously co-transfected with Gaussia luciferase containing the 3′UTRs of IGF1/ NTRK2/ CAMK2B/ ERBB4/ ANAPC11 and Firefly luciferase cloned in pMIR-Report plasmid as well as pRLTK. Luciferase activities were measured 48 hrs post transfection. Dual Luciferase Reporter Assay System (Promega) was used to measure the intensities of Gaussia and Firefly luciferases. Data was analyzed as the ratio of intensities from Gaussia luciferase to Firefly luciferase.

AAV Preparation and Stereotaxic Injection into arcuate nucleus:

Adenovirus was produced by cotransfection of 9.55 µgm of empty plasmid (expressing tdTomato by CAG promoter) or sponge plasmid (tdTomato with the sponge sequence inserted in the ORF under the CAG promoter), 9.55 µgm pAAV2/9n and 19.22 µgm pAdDeltaF6 in HEK293T cells. Calcium phosphate method of transfection was used to deliver the plasmids to HEK293T cells. Cells were incubated in low glucose DMEM media (Gibco) with 10% fetal bovine serum and maintained at 5% CO_2 and 37°C. 72 hours after transfection, media was collected and the cells were lysed and filtered with a 100-micron filter mesh. The media and lysed cells were pooled and viral pellets were obtained using ultracentrifugation. Viral particles were resuspended in 1X PBS with 5% Glycerol.

Stereotaxic surgeries were performed on the animals to deliver the AAV containing miRNA sponge to the arcuate nucleus as mentioned above. Using a hamilton syringe, 200 nL of the AAVs were injected into the arcuate nucleus at the stereotaxic coordinates (Anterior -0.02 cm; Lateral -0.002 cm; Ventral -0.059 cm; w.r.t Bregma). After the surgery, animals were allowed to recover for 10-12 days before the feeding and injections were started.

Confocal Imaging and Image Analysis:

Brain sections stained and mounted were imaged using a Nikon A1 HD25 point scanning microscope with a Nikon 20X Objective at a 1024*1024 resolution of pixels. Optical sections of 1µm step sizes were captured for the entire brain sections. All captured images were of 16-bit pixel depth, and had uniform laser power, detector gain and pinhole diameter values.

TIFFs of raw images were selected from all channels expressing DAPI, BrdU, POMC, AgRP, c-fos and NeuN. Using custom written MATLAB algorithms, all images were thresholded dynamically with their respective background noise. Thresholded images at the same optical section depths were used to quantify the underlying number of cells expressing in each channel as well as the number of colocalization between the channels. The data was then exported, pooled, analyzed and plotted for significance.

miRNA Sponge Efficacy Analysis:

Primary neuronal cultures were prepared from dissected mouse embryonic (E17) cortices as described previously (*48*). About 160 to 170 cells/mm^2 were plated for verifying the efficacy of miRNA sponge expression. Neurons were grown *in vitro* in Neurobasal medium (Gibco) containing B27 supplements (Gibco) at 5% CO_2/37°C. Adenoviruses expressing miRNA sponge or empty sponge vectors were transduced at DIV (days *in vitro*) 7. Neurons were fixed with 4% paraformaldehyde at DIV 21 and were counterstained with DAPI containing media.

Neurons were imaged using a Nikon A1 HD25 point scanning microscope with a Nikon 100X Objective at a 1024*1024 resolution of pixels. Optical sections of 0.2 µm step sizes were captured for the entire neuron. All captured images were of 16-bit pixel depth, and had uniform laser power, detector gain and pinhole diameter values.

Maximum Intensity Projections of each neuron were made as TIFFs from raw images and the average global pixel intensities of tdTomato fluorescence were computed using Matlab. The data was collected and pooled for statistical analysis.

Statistics:

Statistical analysis was performed for all experiments. miRNA differential expressions were analyzed for significance using two-tailed students' t-test and post hoc determination of false discovery rates using the Benjamini-Hochberg method (*49*). Luciferase reporter assays and intensity analysis for miRNA sponge expression were analyzed for significance using unpaired two-tailed t-test with Welch's correction. One-way ANOVA and multiple comparison using Fisher's least significant difference was performed to analyze the significance for quantitation of c-Fos co-expression in BrdU$^+$ neurons. Unpaired t-test with Welch's correction was used to determine the significance for determination of orexigenic and anorexigenic fate and their functional activity in the neural circuit.

References

1. M. V. Kokoeva, H. Yin, J. S. Flier, Evidence for constitutive neural cell proliferation in the adult murine hypothalamus. *J. Comp. Neurol.* **505** (2007).

2. D. A. Lee, J. L. Bedont, T. Pak, H. Wang, J. Song, A. Miranda-Angulo, V. Takiar, V. Charubhumi, F. Balordi, H. Takebayashi, S. Aja, E. Ford, G. Fishell, S. Blackshaw, Tanycytes of the hypothalamic median eminence form a diet-responsive neurogenic niche. *Nat. Neurosci.* **15** (2012).

3. P. J. Enriori, A. E. Evans, P. Sinnayah, E. E. Jobst, L. Tonelli-Lemos, S. K. Billes, M. M. Glavas, B. E. Grayson, M. Perello, E. A. Nillni, K. L. Grove, M. A. Cowley, Diet-Induced Obesity Causes Severe but Reversible Leptin Resistance in Arcuate Melanocortin Neurons. *Cell Metab.* **5** (2007).

4. D. I. Briggs, S. H. Lockie, Q. Wu, M. B. Lemus, R. Stark, Z. B. Andrews, Calorie-restricted weight loss reverses high-fat diet-induced ghrelin resistance, which contributes to rebound weight gain in a ghrelin-dependent manner. *Endocrinology* **154** (2013).

5. D. A. Lee, S. Yoo, T. Pak, J. Salvatierra, E. Velarde, S. Aja, S. Blackshaw, Dietary and sex-specific factors regulate hypothalamic neurogenesis in young adult mice. *Front. Neurosci.*, doi: 10.3389/fnins.2014.00157 (2014).

6. S. Yoo, S. Blackshaw, Regulation and function of neurogenesis in the adult mammalian hypothalamus. Elsevier Ltd (2018). https://doi.org/10.1016/j.pneurobio.2018.04.001.

7. T. C. Mathew, Regional analysis of the ependyma of the third ventricle of rat by light and electron microscopy. *J. Vet. Med. Ser. C Anat. Histol. Embryol.* **37** (2008).

8. M. A. Cowley, J. L. Smart, M. Rubinstein, M. G. Cerdán, S. Diano, T. L. Horvath, R. D. Cone, M. J. Low, Leptin activates anorexigenic POMC neurons through a neural network in the arcuate nucleus. *Nature* **411** (2001).

9. Y. Aponte, D. Atasoy, S. M. Sternson, AGRP neurons are sufficient to orchestrate feeding behavior rapidly and without training. *Nat. Neurosci.* **14** (2011).

10. J. W. Sohn, Network of hypothalamic neurons that control appetite. (2015). https://doi.org/10.5483/BMBRep.2015.48.4.272.

11. S. Sangiao-Alvarellos, L. Pena-Bello, M. Manfredi-Lozano, M. Tena-Sempere, F. Cordido, Perturbation of Hypothalamic MicroRNA Expression Patterns in Male Rats After Metabolic Distress: Impact of Obesity and Conditions of Negative Energy Balance. *Endocrinology* **155**, 1838–1850 (2014).

12. I. A. Vinnikov, K. Hajdukiewicz, J. Reymann, J. Beneke, R. Czajkowski, L. C. Roth, M. Novak, A. Roller, N. Dorner, V. Starkuviene, F. J. Theis, H. Erfle, G. Schutz, V. Grinevich, W. Konopka, Hypothalamic miR-103 Protects from Hyperphagic Obesity in Mice. *J. Neurosci.* **34**, 10659–10674 (2014).

13. L. Stappert, F. Klaus, O. Brüstle, MicroRNAs engage in complex circuits regulating adult neurogenesis. (2018). https://doi.org/10.3389/fnins.2018.00707.

14. M. A. Lopez-Ramirez, S. Nicoli, Role of miRNAs and epigenetics in neural stem cell fate determination. *Epigenetics* **9**, 90–100 (2014).

15. X. Tang, G. Tang, S. Özcan, Role of microRNAs in diabetes. (2008). https://doi.org/10.1016/j.bbagrm.2008.06.010.

16. P. Bielefeld, A. Sierra, J. M. Encinas, M. Maletic-Savatic, A. Anderson, C. P. Fitzsimons, A standardized protocol for stereotaxic intrahippocampal administration of kainic acid combined with electroencephalographic seizure monitoring in mice. *Front. Neurosci.* **11** (2017).

17. J. G. Maldonado-Avilés, D. J. Guarnieri, X. Zhu, R. J. DiLeone, Down-regulation of miRNAs in the brain and development of diet-induced obesity. *Int. J. Dev. Neurosci.* **64** (2018).

18. F. Zhang, D. Ma, W. Zhao, D. Wang, T. Liu, Y. Liu, Y. Yang, Y. Liu, J. Mu, B. Li, Y. Zhang, Y. Pan, C. Guo, H. Du, L. Li, X. Fu, Z. Cao, L. Jin, Obesity-induced overexpression of miR-802 impairs insulin transcription and secretion. *Nat. Commun.* **11** (2020).

19. M. Porniece Kumar, A. L. Cremer, P. Klemm, L. Steuernagel, S. Sundaram, A. Jais, A. C. Hausen, J. Tao, A. Secher, T. Å. Pedersen, M. Schwaninger, F. T. Wunderlich, B. B. Lowell, H. Backes, J. C. Brüning, Insulin signalling in tanycytes gates hypothalamic insulin uptake and regulation of AgRP neuron activity. *Nat. Metab.* **3** (2021).

20. M. Rubinov, O. Sporns, Complex network measures of brain connectivity: Uses and interpretations. *Neuroimage* **52**, 1059–1069 (2010).

21. J. Song, K. M. Christian, G. L. Ming, H. Song, Modification of hippocampal circuitry by adult neurogenesis. *Dev. Neurobiol.* **72**, 1032–1043 (2012).

22. D. Lim, A. Alvarez-Buylla, The Adult Ventricular – Subventricular Zone and Olfactory bulb Neurogenesis. *Cold Spring Harb. Perspect. Biol.* **8**, a018820 (2016).

23. M. V. Kokoeva, H. Yin, J. S. Flier, Neurogenesis in the hypothalamus of adult mice: Potential role in energy balance. *Science (80-.).* **310** (2005).

24. E. M. Rodríguez, J. L. Blázquez, F. E. Pastor, B. Peláez, P. Peña, B. Peruzzo, P. Amat, Hypothalamic tanycytes: A key component of brain-endocrine interaction. *Int. Rev. Cytol.* **247**, 89–164 (2005).

25. C. Esau, S. Davis, S. F. Murray, X. X. Yu, S. K. Pandey, M. Pear, L. Watts, S. L. Booten, M. Graham, R. McKay, A. Subramaniam, S. Propp, B. A. Lollo, S. Freier, C. F. Bennett, S. Bhanot, B. P. Monia, miR-122 regulation of lipid metabolism revealed by in vivo antisense targeting. *Cell Metab.* **3** (2006).

26. F. Olivieri, M. Ahtiainen, R. Lazzarini, E. Pöllänen, M. Capri, M. Lorenzi, G. Fulgenzi, M. C. Albertini, S. Salvioli, M. J. Alen, U. M. Kujala, G. Borghetti, L. Babini, J. Kaprio, S. Sipilä, C. Franceschi, V. Kovanen, A. D. Procopio, Hormone replacement therapy enhances IGF-1 signaling in skeletal muscle by diminishing miR-182 and miR-223 expressions: A study on postmenopausal monozygotic twin pairs. *Aging Cell* **13** (2014).

27. L. Jean-François, A. Derghal, L. Mounien, Micrornas in obesity and related metabolic disorders. *Cells* **8** (2019).

28. A. Kozomara, M. Birgaoanu, S. Griffiths-Jones, MiRBase: From microRNA sequences to function. *Nucleic Acids Res.* **47**, D155–D162 (2019).

29. D. Aberg, Role of the growth hormone/insulin-like growth factor 1 axis in neurogenesis. (2009). https://doi.org/10.1159/000262529.

30. M. A. I. Åberg, N. D. Åberg, H. Hedbäcker, J. Oscarsson, P. S. Eriksson, Peripheral Infusion of IGF-I Selectively Induces Neurogenesis in the Adult Rat Hippocampus. *J. Neurosci.* **20**, 2896–2903 (2000).

31. G. J. F. Brooker, M. Kalloniatis, V. C. Russo, M. Murphy, G. A. Werther, P. F. Bartlett, Endogenous IGF-1 regulates the neuronal differentiation of adult stem cells. *J. Neurosci. Res.* **59**, 332–341 (2000).

32. D. D. Bikle, C. Tahimic, W. Chang, Y. Wang, A. Philippou, E. R. Barton, Role of IGF-I signaling in muscle bone interactions. (2015). https://doi.org/10.1016/j.bone.2015.04.036.

33. J. Gray, G. Yeo, C. Hung, J. Keogh, P. Clayton, K. Banerjee, A. McAulay, S. O'Rahilly, I. S. Farooqi, Functional characterization of human NTRK2 mutations identified in patients with severe early-onset obesity. *Int. J. Obes.* **31** (2007).

34. B. Xu, E. H. Goulding, K. Zang, D. Cepoi, R. D. Cone, K. R. Jones, L. H. Tecott, L. F. Reichardt, Brain-derived neurotrophic factor regulates energy balance downstream of melanocortin-4 receptor. *Nat. Neurosci.* **6** (2003).

35. F. F. Hamdan, C. T. Myers, P. Cossette, P. Lemay, D. Spiegelman, A. D. Laporte, C. Nassif, O. Diallo, J. Monlong, M. Cadieux-Dion, S. Dobrzeniecka, C. Meloche, K. Retterer, M. T. Cho, J. A. Rosenfeld, W. Bi, C. Massicotte, M. Miguet, L. Brunga, B. M. Regan, K. Mo, C. Tam, A. Schneider, G. Hollingsworth, D. R. FitzPatrick, A. Donaldson, N. Canham, E. Blair, B. Kerr, A. E. Fry, R. H. Thomas, J. Shelagh, J. A. Hurst, H. Brittain, M. Blyth, R. R. Lebel, E. H. Gerkes, L. Davis-Keppen, Q. Stein, W. K. Chung, S. J. Dorison, P. J. Benke, E. Fassi, N. Corsten-Janssen, E. J. Kamsteeg, F. T. Mau-Them, A. L. Bruel, A. Verloes, K. Õunap, M. H. Wojcik, D. V. F. Albert, S. Venkateswaran, T. Ware, D. Jones, Y. C. Liu, S. S. Mohammad, P. Bizargity, C. A. Bacino, V. Leuzzi, S. Martinelli, B. Dallapiccola, M. Tartaglia, L. Blumkin, K. J. Wierenga, G. Purcarin, J. J. O'Byrne, S. Stockler, A. Lehman, B. Keren, M. C. Nougues, C. Mignot, S. Auvin, C. Nava, S. M. Hiatt, M. Bebin, Y. Shao, F. Scaglia, S. R. Lalani, R. E. Frye, I. T. Jarjour, S. Jacques, R. M. Boucher, E. Riou, M. Srour, L. Carmant, A. Lortie, P. Major, P. Diadori, F. Dubeau, G. D'Anjou, G. Bourque, S. F. Berkovic, L. G. Sadleir, P. M. Campeau, Z. Kibar, R. G. Lafrenière, S. L. Girard, S. Mercimek-Mahmutoglu, C. Boelman, G. A. Rouleau, I. E. Scheffer, H. C. Mefford, D. M. Andrade, E. Rossignol, B. A. Minassian, J. L. Michaud, High Rate of Recurrent De Novo Mutations in Developmental and Epileptic Encephalopathies. *Am. J. Hum. Genet.* **101** (2017).

36. K. A. Miller, S. R. F. Twigg, S. J. McGowan, J. M. Phipps, A. L. Fenwick, D. Johnson, S. A. Wall, P. Noons, K. E. M. Rees, E. A. Tidey, J. Craft, J. Taylor, J. C. Taylor, J. A. C. Goos, S. M. A. Swagemakers, I. M. J. Mathijssen, P. J. van der Spek, H. Lord, T. Lester, N. Abid, D. Cilliers, J. A. Hurst, J. E. V. Morton, E. Sweeney, A. Weber, L. C. Wilson, A. O. M. Wilkie, Diagnostic value of exome and whole genome sequencing in craniosynostosis. *J. Med. Genet.* **54** (2017).

37. A. J. Rose, B. Kiens, E. A. Richter, Ca2+-calmodulin-dependent protein kinase expression and signalling in skeletal muscle during exercise. *J. Physiol.* **574** (2006).

38. R. A. G. Garcia, K. Vasudevan, A. Buonanno, The neuregulin receptor ErbB-4 interacts with PDZ-containing proteins at neuronal synapses. *Proc. Natl. Acad. Sci. U. S. A.* **97** (2000).

39. Y. Z. Huang, S. Won, D. W. Ali, Q. Wang, M. Tanowitz, Q. S. Du, K. A. Pelkey, D. J. Yang, W. C. Xiong, M. W. Salter, L. Mei, Regulation of neuregulin signaling by PSD-95 interacting with ErbB4 at CNS synapses. *Neuron* **26** (2000).

40. S. Jessberger, G. Kempermann, Adult-born hippocampal neurons mature into activity-dependent responsiveness. *Eur. J. Neurosci.* **18** (2003).

41. D. M. Kokare, G. P. Shelkar, C. D. Borkar, K. T. Nakhate, N. K. Subhedar, A simple and inexpensive method to fabricate a cannula system for intracranial injections in rats and mice. *J. Pharmacol. Toxicol. Methods* **64**, 246–250 (2011).

42. V. Agarwal, G. W. Bell, J.-W. Nam, D. P. Bartel, Predicting effective microRNA target sites in mammalian mRNAs. *Elife* **4** (2015).

43. W. Liu, X. Wang, Prediction of functional microRNA targets by integrative modeling of microRNA binding and target expression data. *Genome Biol.* **20**, 1–10 (2019).

44. Y. Chen, X. Wang, MiRDB: An online database for prediction of functional microRNA targets. *Nucleic Acids Res.* **48**, D127–D131 (2020).

45. A. Krek, D. Grün, M. N. Poy, R. Wolf, L. Rosenberg, E. J. Epstein, P. MacMenamin, I. Da Piedade, K. C. Gunsalus, M. Stoffel, N. Rajewsky, Combinatorial microRNA target predictions. *Nat. Genet.* **37**, 495–500 (2005).

46. M. S. Ebert, J. R. Neilson, P. A. Sharp, MicroRNA sponges: Competitive inhibitors of small RNAs in mammalian cells. *Nat. Methods* **4** (2007).

47. J. Kluiver, I. Slezak-Prochazka, K. Smigielska-Czepiel, N. Halsema, B. J. Kroesen, A. van den Berg, Generation of miRNA sponge constructs. *Methods* **58** (2012).

48. S. Kaech, G. Banker, Culturing hippocampal neurons. *Nat. Protoc.* **1**, 2406–2415 (2006).

49. Y. Benjamini, Y. Hochberg, Controlling the False Discovery Rate: A Practical and Powerful Approach to Multiple Testing. *J. R. Stat. Soc. Ser. B* **57**, 289–300 (1995).

Acknowledgments

We thank Addgene for AAV vectors. We thank Ananya Ghosh and Santhosh Kumar for the technical assistance.

Funding:

This study was funded by the Department of Biotechnology, Government of India (BT/PR8793/AGR/36/749/2013) and NBRC core fund to Sourav Banerjee.

Supplementary Figures:

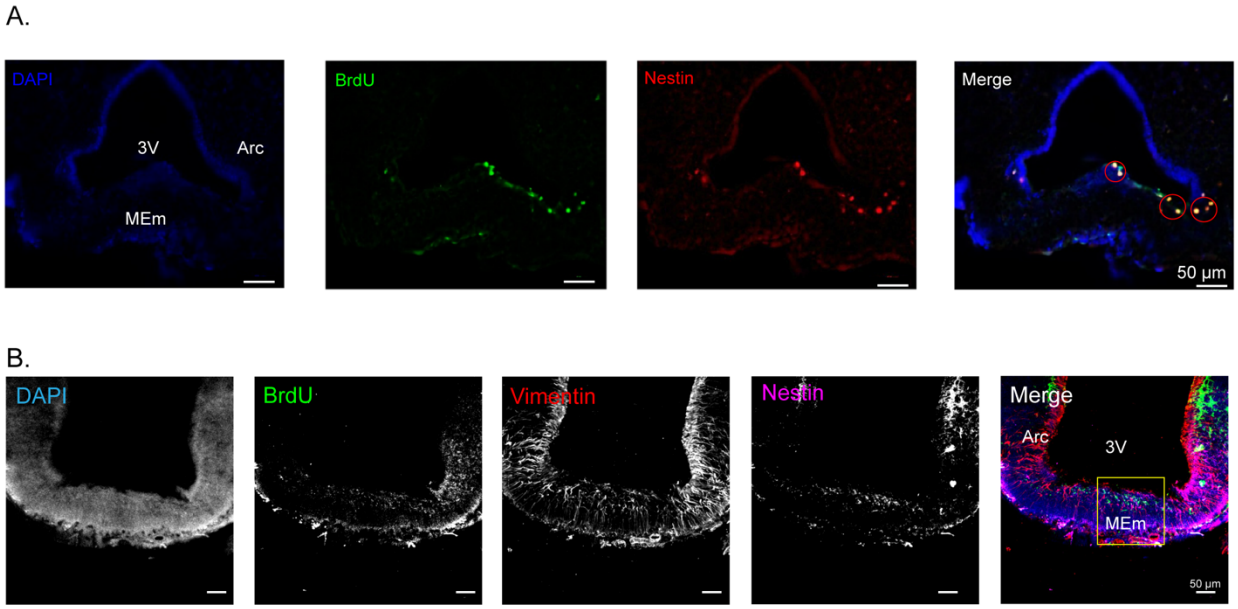

Figure S1: BrdU labelling of neurogenic tanycytes in median eminence (MEm) of hypothalamus upon HFD feeding.

(A) Photomicrograph showing $BrdU^+$ co-labelled with Nestin, a neurogenic marker. $BrdU^+$ tanycytes marked in "red" circle were laser captured for miRNA array. (B) Photomicrograph showing BrdU labelled $Vimentin^+$ neurogenic tanycytes. Arc: Arcuate Nucleus, 3V: Third ventricle. Scale as indicated.

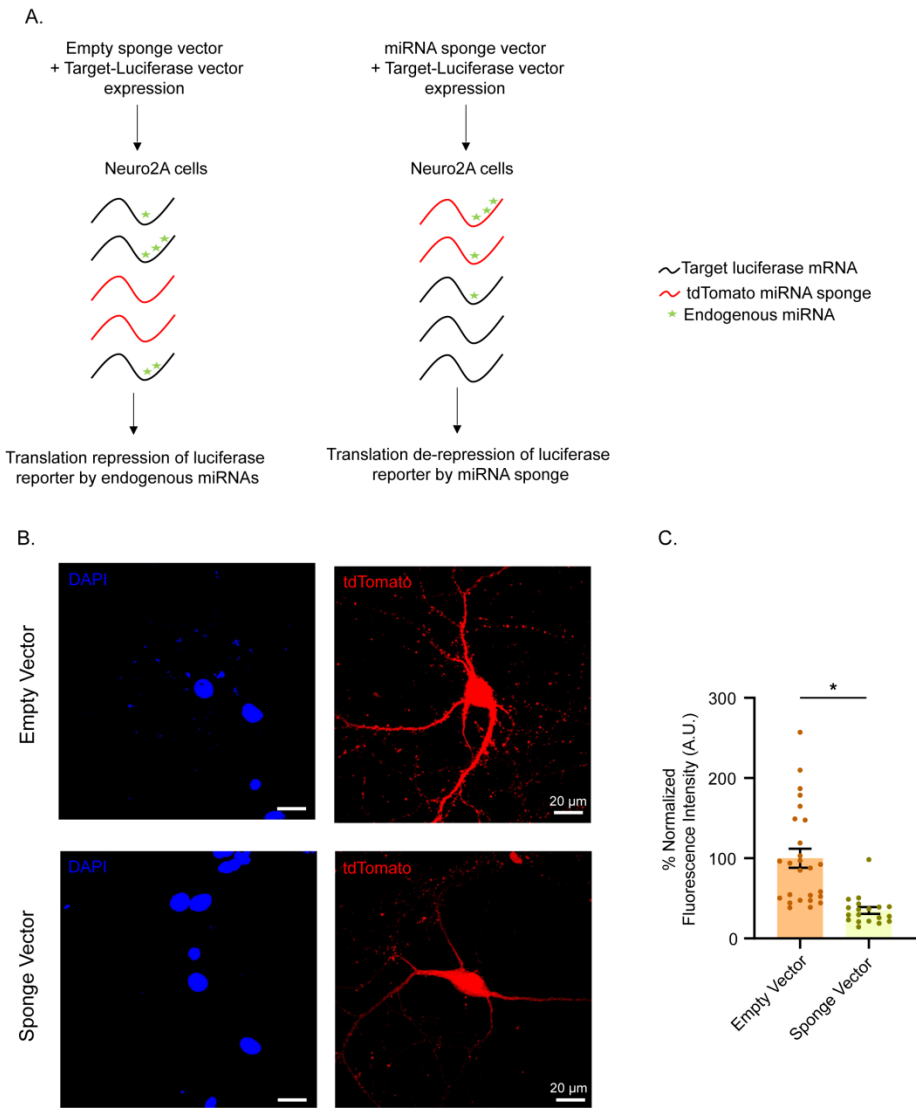

Figure S2: Inhibition of diet-regulated miRNA by sponge

(A) Schematic for miRNA sponge-mediated inhibition of miRNA-mRNA target interaction as measured by reporter assay. (B). Photomicrograph representing miRNA sponge activity in primary cortical neurons following AAV-mediated miRNA sponge expression. Scale as indicated. (C) Quantitation of inhibition of tdTomato expression by miRNA sponge in primary cortical neuron. N = 19 – 26 neurons from 3 independent experiments. *p<0.0001. Two-tailed t-test with Welch's correction. Data shown as mean ± SEM.

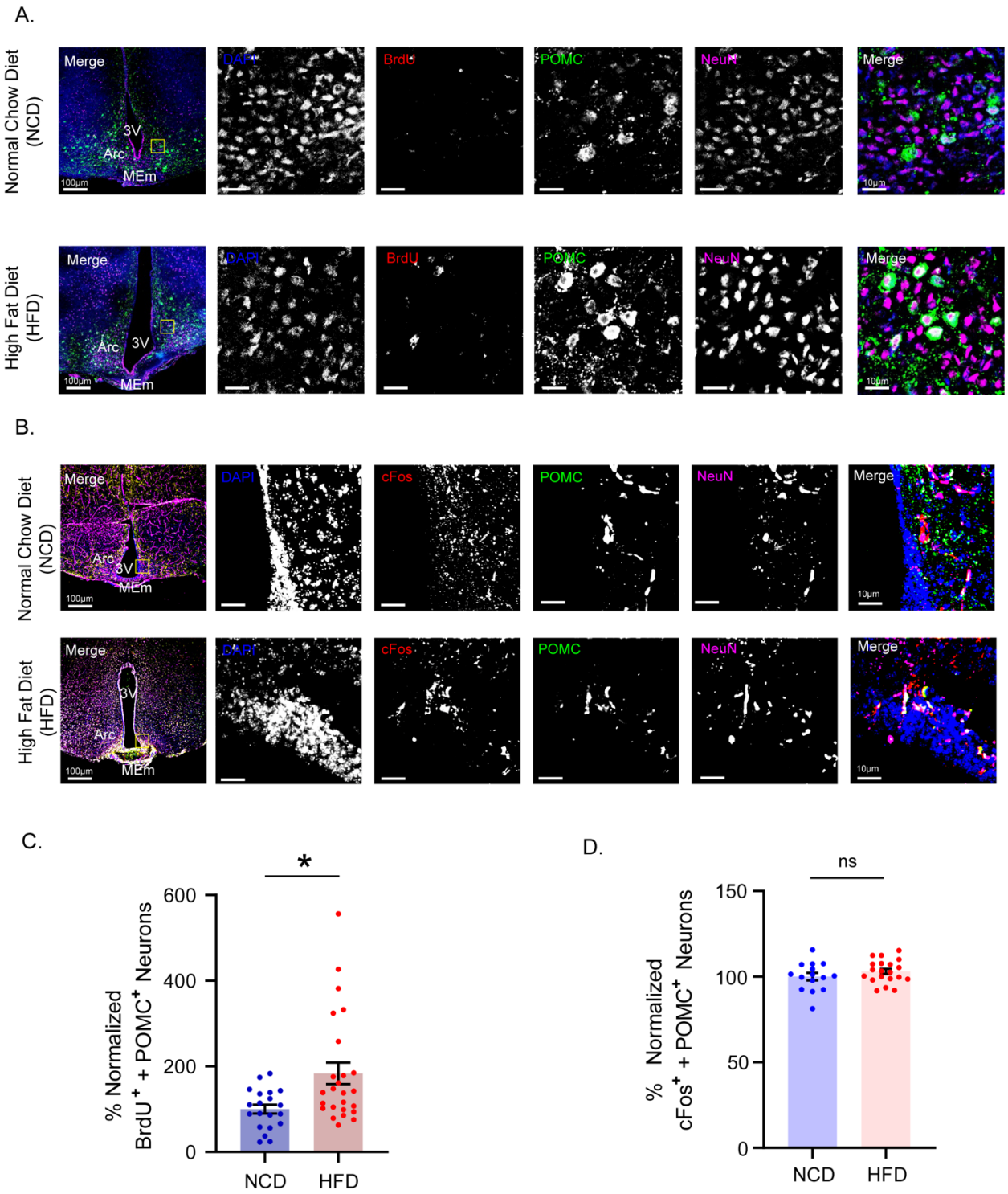

Figure S3: Diet-induced newborn POMC neurons are not functionally active.

(A) Photomicrographs represent anorexigenic fate of diet-induced nascent neurons upon HFD or NCD feeding. Low magnification image of brain sections of all channels [DAPI (blue), BrdU (red), POMC (green), NeuN (magenta)] were merged (white). High

magnification images of brain sections labelled with DAPI (blue), BrdU (red), POMC (green), NeuN (magenta) and merged (white). Scale bars are indicated. (B) Photomicrographs showing POMC neurons without functional activity upon HFD or NCD feeding. Low magnification image of brain sections of all channels [DAPI (blue), c-Fos (red), POMC (green), NeuN (magenta)] were merged (white). High magnification images of brain sections labelled with DAPI (blue), c-Fos (red), POMC (green), NeuN (magenta) and merged (white). Scale bars are indicated. (C) Quantitation of normalized $BrdU^+$ and $POMC^+$ neurons. Data is shown as mean ± SEM. N = 20 - 25 brain sections from 3 independent experiments. Two-tailed t-test with Welch's correction. (D) Quantitation of normalized $c\text{-}Fos^+$ and $POMC^+$ neurons. Scale bars are indicated. Data shown as mean ± SEM. N = 15-20 brain sections from 3 independent experiments. Two-tailed t-test with Welch's correction.